2015

Spark Discharge Coupled Laser Multicharged Ion Source

Md. Haider A. Shaim
Old Dominion University

Hani E. Elsayed-Ali
Old Dominion University, helsayed@odu.edu

Original Publication Citation

Shaim, M. H. A., & Elsayed-Ali, H. E. (2015). Spark discharge coupled laser multicharged ion source. *Review of Scientific Instruments, 86*(7), 073304. doi:10.1063/1.4923457

Spark discharge coupled laser multicharged ion source

Md. Haider A. Shaim and Hani E. Elsayed-Ali[a)]
Department of Electrical and Computer Engineering and the Applied Research Center, Old Dominion University, Norfolk, Virginia 23529, USA

(Received 25 April 2015; accepted 22 June 2015; published online 7 July 2015)

A spark discharge is coupled to a laser multicharged ion source to enhance ion generation. The laser plasma triggers a spark discharge with electrodes located in front of the ablated target. For an aluminum target, the spark discharge results in significant enhancement in the generation of multicharged ions along with higher charge states than observed with the laser source alone. When a Nd:YAG laser pulse (wavelength 1064 nm, pulse width 7.4 ns, pulse energy 72 mJ, laser spot area on target 0.0024 cm^2) is used, the total multicharged ions detected by a Faraday cup is 1.0 nC with charge state up to Al^{3+}. When the spark amplification stage is used (0.1 μF capacitor charged to 5.0 kV), the total charge measured increases by a factor of ~9 with up to Al^{6+} charge observed. Using laser pulse energy of 45 mJ, charge amplification by a factor of ~13 was observed for a capacitor voltage of 4.5 kV. The spark discharge increases the multicharged ion generation without increasing target ablation, which solely results from the laser pulse. This allows for increased multicharged ion generation with relatively low laser energy pulses and less damage to the surface of the target. © *2015 AIP Publishing LLC.* [http://dx.doi.org/10.1063/1.4923457]

I. INTRODUCTION

Multicharged ions (MCIs) sources are of interest for their utilization in surface modification, e.g., etching and deposition, for ion implantation and for fundamental studies of ion-surface interactions. The interaction of MCIs with solids is different from that of singly charged ions. For singly charged ions, the ion projectile mainly interacts with the target nuclei causing surface sputtering, intermixing, and defect generation.[1] The total energy of an ion beam depends on the charge state of the ions (potential energy) and its velocity (kinetic energy). During interaction with a solid, the potential energy carried by the MCIs is released along with its kinetic energy. This potential energy can be significant for highly charged ions and can exceed that of the ion kinetic energy. The release of the ion potential energy causes electronic exchange interaction in the target material and electronic excitation.[2] For sufficiently slow MCI, this released potential energy can be localized to a depth of few nanometers causing surface nano-features. The ability to select potential and kinetic energy of the MCI makes MCI sources an important tool for nanotechnology, microelectronics, and semiconductor processing.

One attractive application of MCIs is ion implantation. MCIs can allow for ion implantation at different depths in a single step since different charge states are accelerated to different kinetic energies with the same potential.[3] Also, the ability to control both kinetic and potential energy of the MCIs could possibly be used to minimize implantation damage by ion recoil.[3] The higher charge state allows reaching higher kinetic energies with lower potential, therefore, reducing the requirement on the high voltage power supply making it possible to develop comparatively low-cost and compact ion implanter.

Multicharged ions are mainly generated by electron cyclotron resonance ion sources (ECRIS),[4,5] electron beam ion sources (EBIS),[6,7] and laser multicharged ion (LMCI) sources.[8,9] ECRIS and EBIS operate only with gases and, therefore, for elements with low vapor pressures, they require introducing gaseous compounds or some vaporization mechanism. Introduction of gases inside the MCI system requires additional pumping capacity to avoid recombination of the MCIs in the generation chamber and the transport beam line. ECRIS and EBIS can produce a continuous beam of MCIs. LMCI sources generate a large number of ions per pulse and can generate MCIs from any solid even from nonconductive or refractory targets.[8,10] LMCI sources can operate in ultrahigh vacuum with a relatively small pumping capacity since no gas load is required for most elements. In principle, LMCI sources can also be used with gas targets since ultrafast laser pulses can induce gas breakdown generating dense plasma.[9] Laser ion sources have been tested as potential ion sources for injection into ion accelerators.[11] Moreover, many pulsed laser deposition systems can be reconfigured into LMCI sources.

In LMCI sources, multicharged ions are generated by focusing a laser pulse on a solid target causing its ablation and ionization. The laser-matter interaction produces dense plasma consisting of ions, electrons, clusters, and neutral particles. The laser plasma plume expands in the perpendicular direction to the ablated surface. The ions are accelerated in the plasma sheath and can be additionally accelerated by an external electric field forming an ion beam.[12–14] LMCI source produces ions from a small spot on the target, which gives control on the ion beam divergence and emittance. The produced MCIs can then be collimated and focused in an ion transport line. Ion charge state selection can be accomplished by electrostatic or magnetic deflectors or by time-of-flight (TOF) pick up with

a)Author to whom correspondence should be addressed. Electronic mail: helsayed@odu.edu. Telephone: (757)269-5645.

deflection plates. Ions with a narrow range of energy-to-charge ratio can be selected with an electrostatic energy analyzer.

Several groups have developed LMCI sources. Abdellatif *et al.* reported that, for aluminum target ablation using a Nd:YAG laser ($\lambda = 1064$ nm, $\tau = 7$ ns and laser intensity of 8.7×10^{10} W cm^{-2}), the plasma density was $\sim 1.13 \times 10^{18}$ cm^{-3} at a distance 100 μm from the Al target surface.[15] At a distance of 1200 μm from the target surface, the plasma density was reduced to 0.55×10^{18} cm^{-3}. The plasma temperature was ~1.17 eV at the target surface, and at a distance of 500 μm, the plasma temperature increased to 4.2 eV then decreased beyond this point. In their experiment, Al charge up to 3+ was generated.[15] Nassisi *et al.* reported on Cu LMCI source with charge state up to 5+ with the majority of ions generated in the singly and doubly charged states with ionization of the plasma estimated to be 16%. In their experiment, an excimer laser providing 70 mJ/pulse, corresponding to 3.5×10^8 W cm^{-2}, was used.[16–18] A Nd:YAG laser ($\lambda = 532$ nm, $\tau = 3$ ns, and maximum energy of 170 mJ/pulse) was used to ablate carbon plasma creating in excess of 70% ionization.[19]

To increase the production of MCIs from LMCI sources, higher plasma density and temperature are needed. This is achieved through the use of larger laser pulse energies, shorter pulse widths, and shorter laser wavelengths to penetrate the formed dense plasma.[20–28] High laser intensity ($\geq 10^{14}$ W cm^{-2}) causes nonlinear interactions, e.g., self-focusing, with the plasma formed by a pre-pulse or the initial part of the laser pulse resulting in higher charge state generation.[20,21] Laska *et al.* observed charge state of >50 for Ta with high kinetic energies (up to 100 keV/amu) using a high power iodine photo-dissociation laser ($\lambda = 1315$ nm, pulse energy 40–750 J, $\tau \sim 400$ ps, intensity $\leq 6 \times 10^{16}$ W cm^{-2}).[20–22] A strong increase in MCI production was observed for laser intensities above $\sim 2 \times 10^{14}$ W cm^{-2} when the laser focus was above the target surface. They also reported on the production of MCIs from different elements by a Nd:YAG laser ($\lambda = 1064$ nm, pulse energy ≤ 0.9 J, pulse width ~9 ns, intensity $\sim 1 \times 10^9$ to $\sim 5 \times 10^{10}$ W cm^{-2}) and an iodine laser (2nd and 3rd harmonic of the fundamental $\lambda = 1310.5$ nm, pulse energy ≤ 50 J, pulse width ~350 ps).[23] For the Nd:YAG laser, which provided low laser intensity, the maximum ion charges reported were Nb^{8+}, Ta^{8+}, W^{9+}, Au^{10+}, and Pb^{9+}. For the iodine laser, the maximum charges observed were Co^{25+}, Ni^{26+}, Ag^{36+}, Sn^{38+}, Ta^{55+}, W^{49+}, Pt^{50+}, Au^{51+}, Pb^{51+}, and Bi^{51+} ion.[23] Lorusso *et al.* used frequency tripled pulses of the iodine laser ($\lambda = 438$ nm, $\tau = 400$ ps, pulse energy ≤ 250 J) to generate up to Ge^{+25} ion.[24] A theoretical model of a hybrid ion source composed of a Nd:YAG laser ($\lambda = 1064$ nm, $\tau = 9$ ns, and maximum pulse energy of 0.9 J) coupled with ECRIS to boost the charge state was developed.[25] These calculations showed that this approach could be effective if the ion energy from the laser source is maintained below a few hundred eV. However, precise control of ion energy in laser ion sources is complicated by ion acceleration in the sheath and plasma shielding effects. In addition, contaminations for the first laser shot can require further outgassing and target etching.[25] Woryna *et al.* reported the generation of up to Ag^{37+} with an iodine laser ($\lambda = 1315$ nm, $\tau = 300$-700 ps, pulse energy ~45 J, intensity $\sim 1 \times 10^{14}$ W cm^{-2}).[26] Using iodine laser ($\lambda = 1315$ nm, pulse width 350-600 ps, pulse energy 40 J, and intensity $\sim 10^{15}$ W cm^{-2}), Rohlena *et al.* reported the generation of charge state up to Ta^{45+} with energies >4 MeV.[27] At CERN, production of high current and high charge state ion beam with maximum charge state of Ta^{23+} was reported using a CO_2 laser ($\lambda = 10.6$ μm, $\tau = 70$ ns, pulse energy ≤ 50 J).[28] Clearly, using lasers with large pulse energies is effective in increasing the plasma density and temperature resulting in higher ionization states and more ion production. However, this approach requires expensive lasers that are typically available only in limited laser laboratories. Therefore, it is desirable to develop LMCI sources capable of delivering high charge states without the complication and cost associated with large laser systems.

We report on the development of a spark discharge coupled laser multicharged ion (SD-LMCI) source to enhance the plasma ionization by depositing spark energy into the laser ablated plume. A similar type of experiment was conducted by Nassef and Elsayed-Ali to enhance the spectral line intensity and signal/background ratio using spark discharge coupled laser induced breakdown spectroscopy.[29] The SD-LMCI source is composed of a laser MCI source and a separate spark stage to deposit energy into the laser ablated plasma. A Q-switched 7.4 ns pulse width Nd:YAG laser is used to ablate Al target. The electrodes of the spark system are placed in front of the Al target and the laser beam is incident on the target through the gap of the electrodes. An accelerating voltage is applied to the target while a grounded mesh is placed in front of the target in order to extract, accelerate, and direct the generated MCIs towards the Faraday cup. The velocity and the charge state of the extracted MCIs are measured using ion TOF as detected by a Faraday cup. The results show that a simple spark discharge, triggered by the laser plasma, can be effectively used to amplify the number of ions produced and increase the ion charge state achieved.

II. EXPERIMENTAL SETUP

A schematic of the SD-LMCI source is shown in Fig. 1. The target is ablated with a Q-switched Nd:YAG laser pulse ($\lambda = 1064$ nm, 7.4 ns pulse width (full-width at half maxima (FWHM)), and pulse energy 72 mJ). The laser beam strikes the Al target surface at an angle $\vartheta = 45°$. The laser beam is focused on the Al surface by a convergent lens with 50 cm focal length. The laser spot area at focus was 0.0024 cm^2, as measured by the knife-edge method at target-equivalent plane with the edge scanned at 45° to the laser beam. The knife edge was used to scan the laser beam in both horizontal and vertical directions. A combination of half-wave plate and thin film polarizer is used to control the focused laser energy on the target. The data reported here were all obtained using a single laser pulse. A 99.9% pure, 0.5 mm thick aluminum disc target (Alfa Aesar) with a surface roughness of 261.77 nm is placed on a multi-axes translational stage. An insulating connector is used to mount the Al target support inside the MCI generation chamber. This arrangement allows applying accelerating voltage directly to the Al target, keeping the experimental chamber at ground. Throughout the experiment, 5 kV bias voltage was applied to the Al target. A nickel mesh of diameter 10-cm,

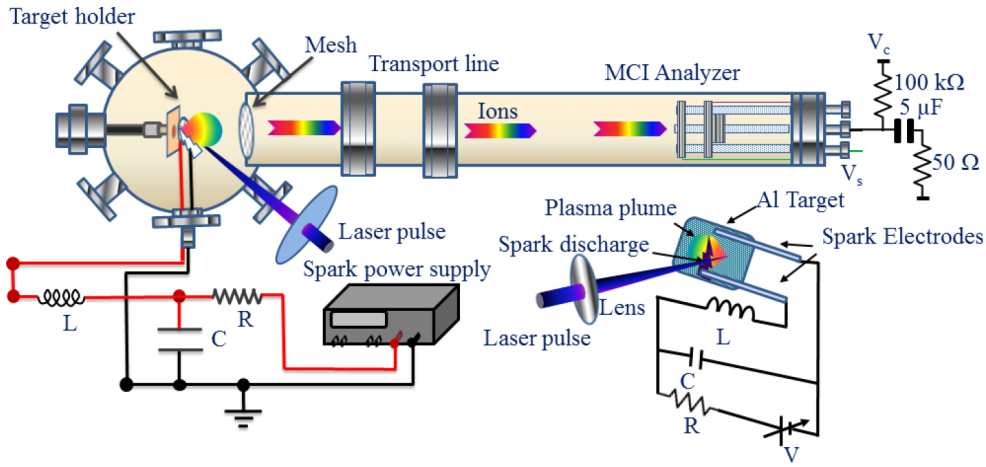

FIG. 1. A schematic of the spark discharge coupled laser multicharged ion (SD-LMCI) source showing the target chamber and a spark system to deposit energy into the plasma plume; V_c is the Faraday cup voltage and V_s is the suppressor voltage. Inset shows the experimental setup used for the spark discharge; C is capacitor, V is voltage applied to the capacitor, R is current limiting resistor, and L is inductor.

thickness of 100 μm, and with an open area of 70% (Precision Eforming) is placed 15-cm in front of the target.

The spark is composed of two parallel Al electrodes of diameter 3.2 mm, separated by ~3 mm, and placed ~5 mm in front of the Al target, as shown in the inset of Fig. 1. The 0.1 μF capacitor is connected to a variable DC power supply through a 5 MΩ current limiting resistor. One of the electrodes is connected to the capacitor through a 0.15 μH inductor. The other electrode is grounded through a 25 cm long wire. The capacitor was charged up to 5 kV. No self-breakdown occurred for these voltages. A high voltage probe (Tektronix P6015A) and a current pick up coil (Pearson Electronics, Inc., 0.001 V/A current monitor) are used to record the voltage drop across the discharge and the discharge current using an oscilloscope. The laser beam strikes the Al sample through the ~3-mm electrode separation. The laser plasma plume expands between the electrodes triggering the spark discharge.

The diameter of the MCI generation chamber is 15 cm. A 125 cm long, 10.2 cm internal diameter (ID) transport tube is connected to the chamber. A Faraday cup of diameter 5 cm made out of Al is placed at the end of the drift tube to collect the MCIs. The interaction of the ions with the Faraday cup emits secondary electrons. To suppress these electrons, a higher negative voltage than the Faraday cup biasing is applied to the suppressor electrode. Throughout the experiment, the Faraday cup voltage was maintained at −70 V and the suppressor electrode voltage was at −110 V. The Faraday cup is connected to the oscilloscope through a capacitor (5 μF), in order to remove the bias voltage from the recorded MCI signal. The MCI system is operating in high vacuum (background pressure in 10^{-7} Torr range) by using a combination of a turbo-molecular pump for initial pumping followed by an ion pump. The total scattering cross section for different MCIs was measured and reported by several groups.[30–32] According to their results, for our experimental condition, the ion travel distance from the Al target to the Faraday cup is much shorter than the mean free path of the generated different MCIs, reducing the MCI loss due to charge transfer with the background gas to a negligible value.

III. RESULTS AND DISCUSSIONS

The spark discharge operation depends on the circuit parameters, separation of the electrodes, electrode distance from target, and the laser ablation plume characteristics.[33,34] The value of the inductor L was adjusted in order to best couple the spark discharge energy to the ablated plume. Fig. 2 shows the voltage measured across the spark discharge (a), current through the discharge (b), and the power dissipated in the plume by the spark (c) when the capacitor C was charged to

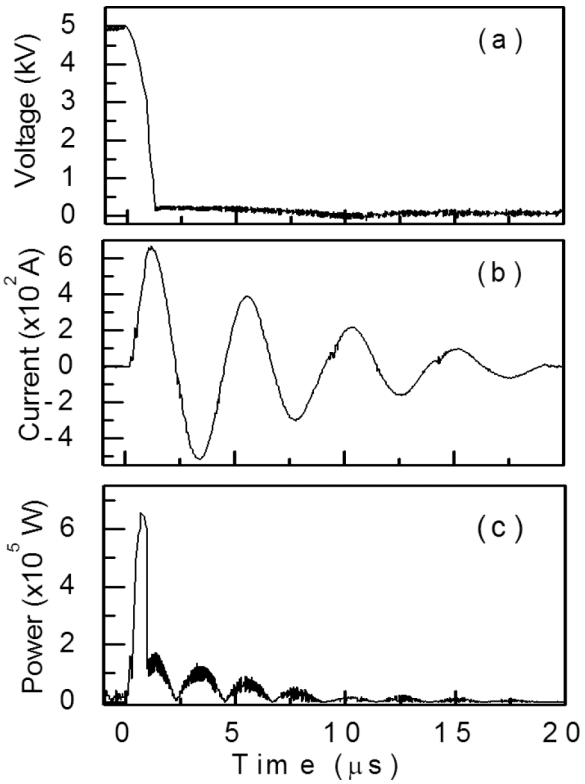

FIG. 2. (a) Voltage measured across the spark electrodes. (b) Discharge current. (c) Deposited electric power in the plasma. The spark was triggered by the Al plasma plume when a 72 mJ laser pulse ablated the Al target. The capacitor C was charged to 5.0 kV.

5.0 kV and a laser energy pulse of 72 mJ was used to ablate the Al target. At this voltage, the total stored energy in C is 1.25 J. As the spark is initiated, the voltage across the two electrodes shows a sudden decay in 1.2 μs. The corresponding current shows damped oscillations with a maximum of ~670 A, as shown in Fig. 2(b). The peak power deposited into the plasma plume is ~0.67 MW, which decays to ~0.1 MW in ~1 μs then oscillates while diminishing with time as shown in Fig. 2(c). Integrating the power dissipating in the discharge, shown in Fig. 2(c), the total energy deposited into the plasma plume is 0.9 J with 0.4 J deposited in 1.0 μs after initiation of the spark discharge. Discharge power dissipation time of ~1 μs or less can best couple the discharge energy with the laser plume and is needed to preserve the shape of the ion signal showing the different ion states separated in time for time-of-flight detection.

The total charge reaching the Faraday cup Q_i is given by $Q_i = \frac{1}{R_L}\int V_F(t)dt$, where $V_F(t)$ is the voltage signal on the Faraday cup and R_L is the 50 Ω internal resistance of the oscilloscope. The process we use to deconvolve the Faraday cup signal into curves for each charge state has been explained in a recent publication on the LMCI source without the spark.[35] The ions, extracted from the plasma plume by the electric field between the target and the grounded mesh, are detected by their TOF signal measured by the Faraday cup. Due to plasma shielding, the ions are not accelerated to the full potential applied between target and grid. The electric field due to the voltage applied to the spark also decelerates the MCIs. If effects due to plasma shielding and the spark electrodes are not considered, an ion generated at the target with zero energy would reach the Faraday cup after a time-of-flight of $TOF = t_a + t_d = \sqrt{\frac{2m}{ZeV}}d + \sqrt{\frac{m}{2ZeV}}S$, where t_a is the time an ion is accelerated from zero velocity at target to velocity v at the extraction mesh, t_d is the time that ions drift at constant velocity v from the extraction mesh to the Faraday cup, d is the distance from the target to the extraction mesh, S is the distance from the extraction mesh to the Faraday cup, m is the mass of Al atom, e is the electron charge, Z is the charge state, and V is the applied accelerating voltage. The above equation does not account for ion acceleration in the plasma which, for our laser parameters, is mainly due to the sheath potential. The ion accelerating time t_a is small compared to the ion drift time t_d. Identifying the charge state from the TOF spectra was performed as follows: Since the Al^{1+} has the lowest velocity, the arrival time of these ions corresponds to the longest TOF. The effective acceleration potential that the Al^{1+} ions were subjected to is obtained by calculating the accelerating voltage required to achieve this TOF for Al^{+1} and applying this accelerating voltage in the above TOF equation. This potential is then used in the TOF equation to determine the TOF of MCIs with other charges. The estimated TOF for MCIs with different charge states matches well the TOF spectra.

A. Effect of spark energy

The TOF ion signals without and with the spark discharge are shown in Fig. 3. The pulse laser energy used was 72 mJ, while the spark discharge was operated at different capacitor C voltages. Without the spark, up to Al^{3+} MCI with a total charge of ~1 nC is detected as shown in Fig. 3(a). When using the same laser pulse energy of 72 mJ and activating the spark by charging the capacitor C to 1.0, 4.0, and 5.0 kV (corresponding to stored energy of 0.05, 0.80, and 1.25 J, respectively), the total charge detected is enhanced and higher charge states are observed. For capacitor voltages of 1.0, 4.0, and 5.0 kV, the total charges generated are 2.0, 6.6, and 9.2 nC, respectively as shown in Figs. 3(b)-3(d). The maximum charge states observed also increase reaching Al^{6+} for V = 5.0 kV. The initial noise in the TOF signal before the arrival of the MCIs to the Faraday cup is due to the spark generated RF noise

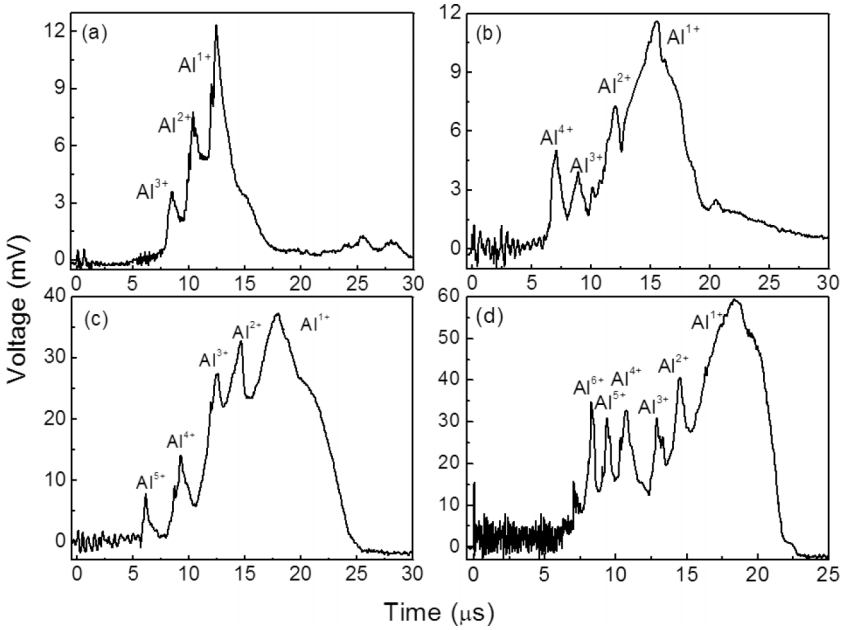

FIG. 3. Spark discharge enhancement of multicharged ion generation for 72 mJ laser energy. (a) Only the laser is used. (b)-(d) Spark discharge operating with energy stored in C of 0.05, 0.80, and 1.25 J, respectively.

that interferes with the signal detected by the Faraday cup.[36] The TOF of the MCIs also shows some peaks with complex shapes, for example, in Fig. 3(d), Al^{3+} and Al^{4+} MCIs show double peaks. The shape of the MCI signal depends on the energy characteristics of the ions which could involve slower and faster ions depending on the ion generation mechanism and the propagation of MCIs through the spark discharge electrodes.[37]

The effect of the spark is to enhance ion generation and increase the maximum ion charge state. By integrating the area under each charge state in Fig. 3, one can determine the abundance of each charge state. From Fig. 3(a), without the spark, the ion charges detected are 72% Al^{1+}, 21% Al^{2+}, and 7% Al^{3+}, while with the spark with C charged at 1.25 J, the ion charges were 56% Al^{1+}, 12% Al^{2+}, 7% Al^{3+}, 11% Al^{4+}, 7% Al^{5+}, and 7% Al^{6+}. The TOF of MCIs is increased when the spark is used since the spark voltage decelerates the extracted ions in the gap between the target and the extraction mesh. In Fig. 4, we show calculation of the most probable energy of the Al^{1+} based on TOF data in Fig. 3. When the laser pulse was used without the spark, the most probable energy of Al^{1+} is ~1.8 keV. As the capacitor C was charged to 1.0, 4.0, and 5.0 kV (corresponding to stored energy of 0.05, 0.80, and 1.25 J, respectively), the most probable energy of Al^{1+} became ~1.1, ~0.9, and ~0.8 keV, respectively. The FWHM of the kinetic energy distribution of Al^{1+} remains unchanged at ~0.6 keV regardless of the spark operating voltage showing that the spark discharge did not introduce additional energy spread in the ion distribution from the laser plasma.

Fig. 5 shows the increase in total charge detected with the increase of energy stored in spark capacitor C. The laser pulse energy is fixed at 72 mJ. We observed that, with the increase of spark energy, total charge generation increased slowly, and for 1.25 J spark energy, the total charge generation increased by a factor of ~9 compared to charge generation with the laser pulse alone. Increasing the spark energy deposited into the laser plasma is expected to increase the plasma density and temperature, which in turn increases the total charge generation.

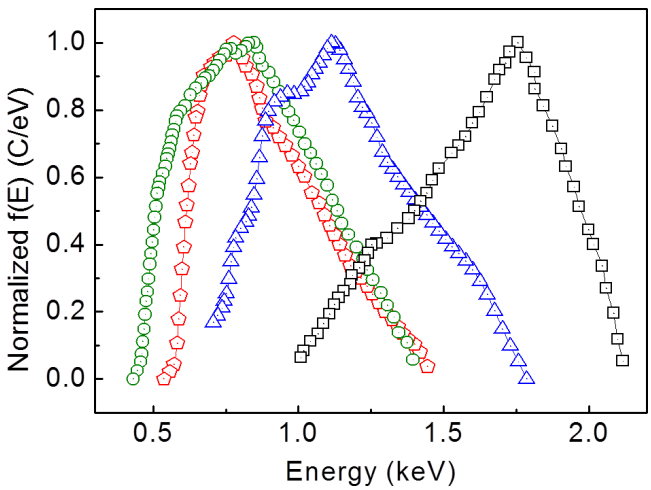

FIG. 4. Energy distribution of Al^{1+} without spark (square) and with spark energy of 0.05 (triangle), 0.8 (circle), and 1.25 J (pentagon) coupled with the 72 mJ laser pulse energy. Spark energy refers to energy stored in C.

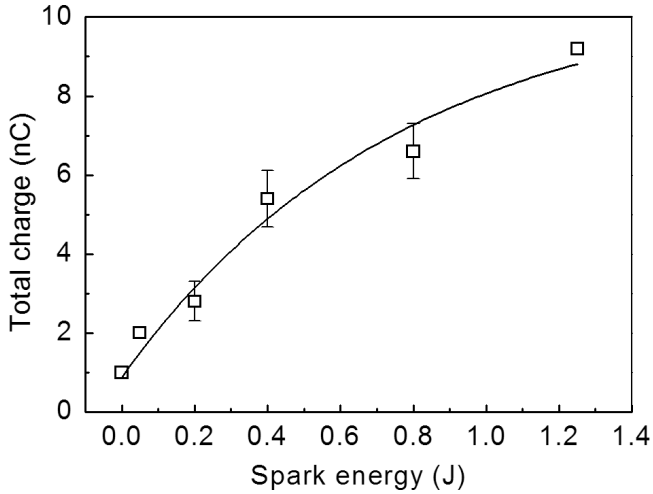

FIG. 5. Effect of spark energy deposited into the plasma plume on total charge detected. Error bars represent standard deviation. Spark energy refers to energy stored in C.

B. Effect of laser energy

In nanosecond laser-matter interaction, an incident laser pulse of sufficient energy causes evaporation of the target surface. Since the pulse width of the nanosecond laser is relatively long, the evaporated materials interact with the remaining part of the laser beam causing progressive ionization of the plasma plume.[38,39] During this process, the electrons are heated by inverse-bremsstrahlung. The heated electrons transfer their energy to the ions and neutrals through collisions. In our experimental conditions, the ablation time is much longer than the time to transfer energy from energetic electrons to ions.[15,40] The lifetime of the laser ablated plume is determined by the velocity of the plume expansion, which in turn is related to the hydrodynamic pressure inside the plume. The average velocity of the plume expansion is affected by the ion mass.[41] In laser ablated plasma, the ablated plasma density, temperature, ablated mass, and the ion, electron energy is affected by the laser pulse energy, intensity, and pulse width. The spark energy deposited into the plasma plume is expected to increase the plasma density and temperature leading to higher ionization rate and higher state charge along with increase in the total number of MCIs generated.

Fig. 6(a) shows the total charge detected for increasing laser energy from 45 to 72 mJ without and with the spark discharge (C charged to 1.00 J). Without the spark, changing the laser pulse energy from 45 to 72 mJ increases the total charge detected from ~0.6 to ~1.0 nC. When 1.00 J spark energy is used in conjunction with the laser pulse, the total charge detected increased from ~8.0 to ~8.3 nC for laser pulse energies of 45 and 72 mJ, respectively. The almost lack of dependence on the laser pulse energy shows that most of the MCIs are generated by the spark discharge energy with the spark causing amplification of the laser-generated MCIs by a factor of ~13 for a laser pulse energy of 45 mJ. Figs. 6(b) and 6(c) show the MCI generation for 45 and 63 mJ laser pulse energy without and with the spark discharge. Without the spark, 45 and 63 mJ laser energies generate Al MCIs with charge states up to Al^{1+} and Al^{3+}, respectively. With a 1.00 J

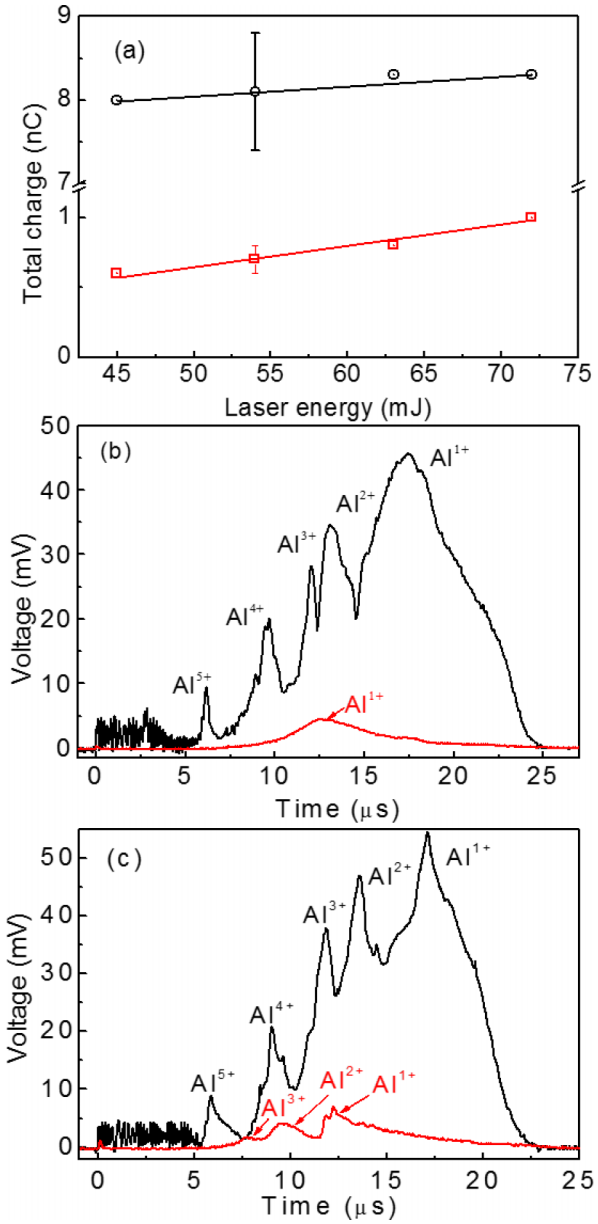

FIG. 6. (a) Measured total charge delivered to the Faraday cup for different laser pulse energies without the spark (squares) and with 1.0 J spark energy (circles). The error bars represent the standard deviation. The MCI spectra for laser energy only (red) and for the combined effect of 1.0 J spark energy and laser pulse energy (black) of (b) 45 and (c) 63 mJ.

spark, MCI charge states up to Al^{+5} are generated for both laser pulse energies. The increased TOF for ions when the spark is operated is due to the ion deceleration by the spark voltage reducing ion kinetic energy. During the experiment, the laser focus spot, angle of incidence on Al target, and pulse width of the laser were kept constant, as described in the experimental section.

IV. CONCLUSION

A spark discharge coupled laser multicharged ion source was developed and tested. A 7.4 ns Nd:YAG laser is used to ablate an Al target generating a plasma plume. The spark discharge is triggered by the laser plume which significantly simplifies the design and provides synchronization of the spark discharge with the laser plume. The spark discharge amplifies the total charge generation and results in higher charge states. The charge state depends mostly on the spark energy deposited rather than on the laser ablation energy. For a laser pulse energy of 72 mJ and spark energy of 1.25 J, charge states up to Al^{6+} were detected. Under this condition, the total charge delivered to the Faraday cup was ~9.2 nC when the target was at 5 kV. The SD-LMCI source is an effective method to generate high charge states of MCIs with small laser pulse energies. This approach also minimizes target damage by the laser pulse since the laser is mainly used to introduce the vapor into the spark while the energy delivered by the spark is used to heat the plasma, which increases the MCI state along with total charge production. The proof-of-concept presented here shows the significant potential of the SD-LMCI source which can be used to generate MCIs out of practically any solid target. Further optimization of the SD-LMCI source is possible by shortening the discharge energy deposition time in the plume to increase the plasma density and temperature. This can be achieved through improvement of the pulse forming network. Also, providing control on discharge trigger time can lead to better coupling of discharge energy with the laser plasma. Other geometries for coupling the discharge energy to the plasma plume and for MCI extraction can also lead to further improvements in MCI yield and energy distribution.

ACKNOWLEDGMENTS

This material is based upon work supported by the National Science Foundation under Grant No. MRI-1228228.

[1]T. Schenkel, A. V. Hamza, A. V. Barnes, and D. H. Schneider, Prog. Surf. Sci. **62**, 23 (1999).
[2]H. Gnaser, Springer Tracts in Modern Physics (Springer, Berlin, Heidelberg, New York, 1999), Vol. 146.
[3]J. D. Gillaspy, J. Phys. B: At., Mol. Opt. Phys. **34**, 93 (2001).
[4]Y. Higurashi, T. Nakagawa, M. Kidera, T. Aihara, K. Kobayashi, M. Kase, A. Goto, and Y. Yano, Rev. Sci. Instrum. **77**, 03A329 (2006).
[5]V. Skalyga, V. Zorin, I. Izotov, S. Razin, A. Sidorov, and A. Bohanov, Plasma Sources Sci. Technol. **15**, 727 (2006).
[6]F. Ullman, F. Grossmann, V. P. Ovsyannikov, J. Gierak, and G. Zschornack, Appl. Phys. Lett. **90**, 083112 (2007).
[7]G. Zschornack, M. Kreller, V. P. Ovsyannikov, F. Grossman, U. Kentsch, M. Schmidt, F. Ullmann, and R. Heller, Rev. Sci. Instrum. **79**, 02A703 (2008).
[8]D. Bleiner, A. Bogaerts, F. Belloni, and V. Nassisi, J. Appl. Phys. **101**, 083301 (2007).
[9]H. Daido, M. Nishiuchi, and A. S. Pirozhkov, Rep. Prog. Phys. **75**, 056401 (2012).
[10]A. Lorusso, L. Velardi, V. Nassisi, F. Paladini, A. M. Visco, N. Campo, L. Torrisi, D. Margarone, L. Giuffrida, and A. Rainò, Nucl. Instrum. Methods Phys. Res., Sect. B **266**, 2490 (2008).
[11]J. Krása, L. Laska, K. Rohlena, M. Pfeifer, J. Skala, B. Kralikova, P. Straka, E. Woryna, and J. Wolowski, Appl. Phys. Lett. **75**, 2539 (1999).
[12]V. Dubenkov, B. Sharkov, A. Golubev, A. Shumshurov, O. Shamaev, I. Roudskoy, A. Streltsov, Y. Satov, K. Makarov, Y. Smakovasky, D. Hoffmann, W. Laus, R. W. Muller, P. Spadtke, C. Stockl, B. Wolf, and J. Jacoby, Laser Part. Beams **14**, 385 (1996).
[13]B. Y. Sharkov, S. Kondrashev, I. Roudskoy, S. Savin, A. Shumshurov, H. Haseroth, H. Kugler, K. Langbein, N. Lisi, H. Magnusson, R. Scrivens, J. C. Schnuringer, J. Tambini, S. Homenko, K. Markov, V. Roerich, A. Stepanov, and Yu. Satov, Rev. Sci. Instrum. **69**, 1035 (1998).
[14]S. Kondrashev, N. Mescheryakov, B. Sharkov, A. Shumshurov, S. Khomenko, K. Makarov, Yu. Satov, and Y. Smakovskii, Rev. Sci. Instrum. **71**, 1409 (2000).
[15]G. Abdellatif and H. Imam, Spectrochim. Acta B **57**, 1155 (2002).

[16]V. Nassisi, A. Pedone, and A. Rainò, Nucl. Instrum. Methods Phys. Res., Sect. B **188**, 267 (2002).
[17]D. Doria, A. Lorusso, F. Belloni, V. Nassisi, L. Torrisi, and S. Gammino, Laser Part. Beams **22**, 461 (2004).
[18]L. Velardi, M. V. Siciliano, D. Delle Side, and V. Nassisi, Rev. Sci. Instrum. **83**, 02B717 (2012).
[19]L. Torrisi, F. Caridi, D. Margarone, A. Picciotto, A. Mangione, and J. J. Beltrano, Appl. Surf. Sci. **252**, 6383 (2006).
[20]L. Láska, K. Jungwirth, J. Krása, M. Pfeifer, K. Rohlena, J. Ullschmied, J. Badziak, P. Parys, J. Wolowski, S. Gammino, L. Torrisi, and F. P. Boody, Appl. Phys. Lett. **86**, 081502 (2005).
[21]Y. Wada, Y. Shigemoto, and A. Ogata, Jpn. J. Appl. Phys., Part 2 **43**, L996 (2004).
[22]L. Laska, K. Jungwirth, J. Krasa, E. KrouskÝ, M. Pfeifer, K. Rohlena, J. Ullschmied, J. Badziak, P. Parys, J. Wolowski, S. Gammino, L. Torrisi, and F. P. Boody, Laser Part. Beams **24**, 175 (2006).
[23]L. Láska, K. Jungwirth, B. Kralikova, J. Krasa, M. Pfeifer, K. Rohlena, J. Skala, J. Ullschmied, J. Badziac, P. Parys, J. Wolowski, E. Woryna, S. Gammino, L. Torrisi, F. P. Boody, and H. Hora, Plasma Phys. Controlled Fusion **45**, 585 (2003).
[24]A. Lorusso, F. Belloni, D. Doria, V. Nassisi, J. Wolowski, J. Badziak, P. Parys, J. Krasa, L. Laska, F. P. Boody, L. Torrisi, A. Mezzasalma, A. Picciotto, S. Gammino, G. Quarta, and D. Bleiner, Nucl. Instrum. Methods Phys. Res., Sect. B **240**, 229 (2005).
[25]S. Gammino, L. Torrisi, L. Andò, G. Ciavola, L. Celona, L. Laska, J. Krasa, M. Pfeifer, K. Rohlena, E. Woryna, J. Wolowski, P. Parys, and G. D. Shirkov, Rev. Sci. Instrum. **73**, 650 (2002).
[26]E. Woryna, J. Wolowski, B. Králiková, J. Krása, L. Laska, M. Pfeifer, K. Rohelna, J. Skala, V. Perina, F. P. Boody, R. Hopfl, and H. Hora, Rev. Sci. Instrum. **71**, 949 (2000).
[27]K. Rohlena, B. Králiková, J. Krása, L. Láska, K. Mašek, M. Pfeifer, J. Skala, J. Farny, P. Parys, J. Wolowski, E. Woryna, W. Mroz, I. Roudskoy, O. Shamaev, B. Sharkov, A. Shumshurov, B. A. Bryunetkin, H. Haseroth, J. Collier, A. Kuttenbeger, K. Langbein, and H. Kugler, Laser Part. Beams **14**, 335 (1996).
[28]H. Haseroth, H. Kugler, K. Langbein, N. Lisi, A. Lombardi, H. Magnusson, W. Pirkl, J. C. Schnuriger, R. Scrivens, J. Tambini, E. Tanke, S. Homenko, K. Makarov, V. Roerich, A. Stepanov, Y. Satov, S. Kondrashev, S. Savin, B. Sharkov, A. Shumshurov, J. Krasa, L. Laska, M. Pfeifer, and E. Woryna, Rev. Sci. Instrum. **69**, 1051 (1998).
[29]O. A. Nassef and H. E. Elsayed-Ali, Spectrochim. Acta B **60**, 1564 (2005).
[30]H. A. Sakaue, K. Hosaka, H. Tawara, I. Yamada, N. Nakamura, S. Ohtani, A. Danjo, M. Kimura, A. Matumoto, M. Sakurai, and M. Yoshino, J. Plasma Fusion Res. **7**, 195 (2006).
[31]H. Ryufuku and T. Watanabe, Phys. Rev. A **20**, 1828 (1979).
[32]D. H. Crandall, R. A. Phaneuf, and F. W. Meyer, Phys. Rev. A **19**, 504 (1979).
[33]P. Persephonis, K. Vlachos, C. Georgiades, and J. Parthenios, J. Appl. Phys. **71**, 4755 (1992).
[34]A. Descoeudres, C. Hollenstein, R. Demellayer, and G. Wälder, J. Mater. Process. Technol. **149**, 184 (2004).
[35]Md. H. A. Shaim and H. E. Elsayed- Ali, Nucl. Instrum. Methods Phys. Res., Sect. B **356-357**, 75 (2015).
[36]M. L. Vestal, Chem. Rev. **101**, 361 (2001).
[37]M. F. Artamonov, V. I. Krasov, and V. L. Paperny, J. Phys. D: Appl. Phys. **34**, 3364 (2001).
[38]S. S. Harilal, B. OShay, M. S. Tillack, and M. V. Mathew, J. Appl. Phys. **98**, 013306 (2005).
[39]A. H. Lutey, J. Appl. Phys. **114**, 083108 (2013).
[40]Y. K. Kim and P. M. Stone, Phys. Rev. A **64**, 052707 (2001).
[41]E. Woryna, P. Parys, and J. Wołowski, Laser Part. Beams **14**, 293 (1996).